



Optics Letters

Few-cycle 12.5-GW pulses generated via efficient all-solid-state post-compression from an ytterbium laser

YUZHE LIU,^{1,2} ZHIDONG CHEN,^{1,2} SENCHI YANG,^{1,2} YICHENG HE,^{1,2} XINBO WANG,^{1,2} YUNFENG MA,³ CHUN ZHOU,⁴ AND SHAOBO FANG^{1,2,*} 

¹Institute of Physics, Chinese Academy of Sciences, Beijing 100190, China

²University of Chinese Academy of Sciences, Beijing 100049, China

³Aerospace Information Research Institute, Chinese Academy of Sciences, Beijing 100094, China

⁴Institute of Plasma Physics, Hefei Institutes of Physical Science, Chinese Academy of Sciences, Hefei 230031, China

*shaobo.fang@iphy.ac.cn

Received 24 September 2024; revised 6 November 2024; accepted 8 November 2024; posted 12 November 2024; published 4 December 2024

In contrast to the more conventional gas-filled post-compression technique, solid-state-based multi-pass cells and multiple plates allow for the robust and efficient generation of intense few-cycle pulses from ytterbium (Yb) lasers with moderate energies. In this Letter, 180-fs 200- μ J pulses at 50 kHz were efficiently compressed down to 6.9 fs 144 μ J, enhancing the peak power from 1.1 GW to 12.5 GW with a long-term power stability of 0.1%. Moreover, we generated over-1.5-octave-spanning white light (500 nm–1420 nm) by using an enhanced self-steepening effect, supporting a Fourier transform limit (FTL) pulse of 2.7 fs (0.8-cycle). © 2024 Optica Publishing Group. All rights, including for text and data mining (TDM), Artificial Intelligence (AI) training, and similar technologies, are reserved.

<https://doi.org/10.1364/OL.542820>

Few- to single-cycle pulse compression technologies have been able to enhance the solid-state extreme ultraviolet (EUV) high harmonic generation (HHG) and isolated attosecond pulse (IAP) emissions [1–3]. These extremely short pulses offer powerful tools for direct tracking and manipulating electrons [4–6] and underlying attosecond dynamics of nonlinear light–matter interactions [7–10]. Using wavelength tunable table-top EUV sources, time- and angle-resolved photoemission spectroscopy (Tr-ARPES) indicate a promising pathway to detect the non-equilibrium electronic structure in solid systems [11,12]. For improving Tr-ARPES measurements, high-flux EUV sources emerging from scalable high-repetition-rate few-cycle pulses are required to reduce the photon number per pulse [13]. In recent years, ytterbium (Yb) lasers provide cost-effective and robust light sources with scalability in high average power and high repetition rates. However, the output pulses directly from Yb lasers are hundreds of femtoseconds due to the gain bandwidth limitation.

To generate extremely short pulses from Yb lasers, 6-m-long 2.2-bar [14] and 1.1-m-long 27-bar [15] gas-filled hollow-core fibers have been applied for pulse compression of a 1-mJ 170-fs Yb laser down to a sub-10-fs regime at 6 kHz. Alternatively,

gas-filled multi-pass cells (MPCs) have been proven to be a good choice for Yb-laser compression [16,17]. Based on argon-filled MPC, compressibility from 112-mJ, 1.3-ps Yb:YAG thin-disk amplifier down to 37 fs has been demonstrated at a repetition rate of 5 kHz [18]. By employing dispersion-engineered dielectric cavity mirrors, gas-filled MPC enabled compression of a 150-fs Yb fiber laser down to sub-20 fs at a 1-kHz repetition rate [19]. For compressing high-repetition-rate (over 50 kHz) Yb lasers with moderate energies, a solid-state post-compression scheme can offer high nonlinear refractive index and provides a space-saving setup. In a single-stage setup, solid-state MPCs are suitable for sub-40-fs pulse compression, reaching a peak power of 0.12 GW at 18.5 MHz [20] and 0.14 GW at 10.6 MHz [21]. Further increasing the input pulse energy, significant milestones have been recorded from single-stage solid-state MPCs with a peak power of 1.1 GW (39 fs [22]), 2.5 GW (31 fs [23]), and 10.2 GW (27 fs [24]). Since the spectral broadening is limited by the ratio between the dispersion length and nonlinear length, multi-stage MPC attempts have been presented to shorten the pulse duration to a sub-20-fs regime. For instance, three-stage solid-state MPCs proved 18-fs, 0.06-GW post-compression [25]. Two-stage solid-state MPCs harvested 22-fs, 0.4-GW [26] and 18-fs, 0.13-GW pulse compression [27]. Recently, by applying a solid-based first MPC stage and an over-8-bar noble-gas-filled second MPC stage, 7-fs, 1-GW [28] and 8-fs, 0.9-GW few-cycle pulses have been achieved with the feasibility of getting close to a sub-two-cycle regime [29]. Meanwhile, double-stage hybrid MPCs with multi-thin plates (MTPs) improved the 8.2-fs source into a 2.9-GW peak power with an overall transmission of 43.5% [30]. Alternatively, the initial double-stage MTPs enabled compression of a 280-fs 400- μ J Yb laser down to an 18-fs 40- μ J source in 2018 [31]. Nowadays, double-stage MTP approaches have been improved to 5.7 fs, 3.9 GW with better thermal management, and the overall efficiency is about 43.9% [32]. To further improve the peak power and pulse duration of a solid-based cascaded compressor, there are opportunities and challenges for combining the advantages of MPC and MTP setups. The approach of the single-stage solid-state MPC and single-stage MTP has been first demonstrated with a sub-30-fs

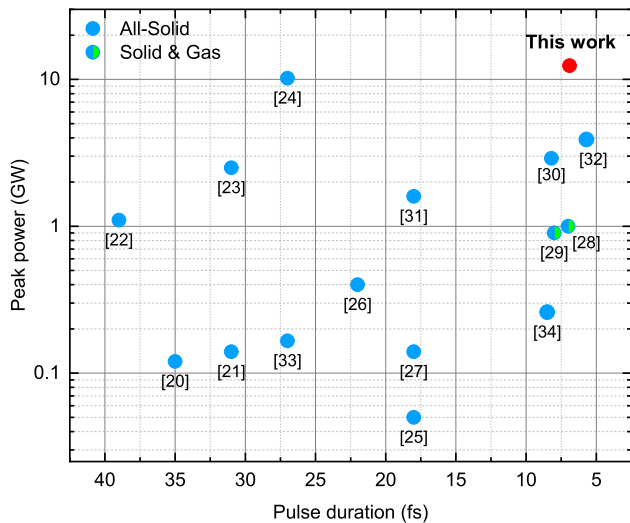


Fig. 1. Overview of the all-solid-state and hybrid post-compression results at 1030 nm for a pulse duration shorter than 50 fs and a repetition rate higher than 50 kHz.

output [33]. By using double-stage solid-state MPCs and single-stage MTP setup, the compressed pulses are further shortened to 8.5 fs [34], however, the peak power is limited at about 0.3 GW. Figure 1 summarizes solid-state post-compression results from Yb lasers for a pulse duration shorter than 50 fs and a repetition rate higher than 50 kHz. It still remains unclear the ability of all-solid-state compressor to efficiently deliver 10-GW few-cycle pulses at high repetition rate.

Here, we demonstrate an all-solid-state 6.9-fs pulse compressor, enhancing the peak power from 1.1 GW to 12.5 GW. The overall transmission of two stages is 72%. Pumped by a Yb:KGW amplifier, the first stage compressed the output pulses from 180 fs down to 18.5 fs with a long-term power stability of 0.04%, very close to Fourier transform limits (FTL) of 18.4 fs. Followed by the second stage, the output pulses are successfully compressed to 6.9 fs with a long-term power stability of 0.1%. The results show a 26-fold overall pulse compression with superior long-term average power stability. Further optimization of white-light generation based on an enhanced self-steepening effect, supercontinuum covering from 500 nm to 1420 nm is generated, supporting an FTL pulse down to 2.7 fs, i.e., 0.8 optical cycle at a center wavelength of 1030 nm.

Figure 2 depicts the schematic of the system layout. The driving laser is an Yb:KGW amplifier (Pharos, Light Conversion), which emits pulses at 50-kHz repetition rates with 10-W average power and 180-fs pulse duration. The first compression stage is based on the MPC in solids. A Galileo system is applied to conduct a mode matching process, the output pulses are guided

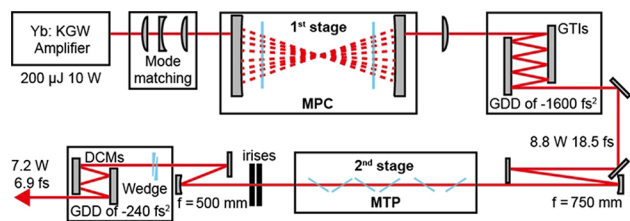


Fig. 2. Schematic diagram of the experimental setup. GTI, Gires–Tournois interferometer mirror; DCM, double chirped mirror; f, focal length of concave mirror.

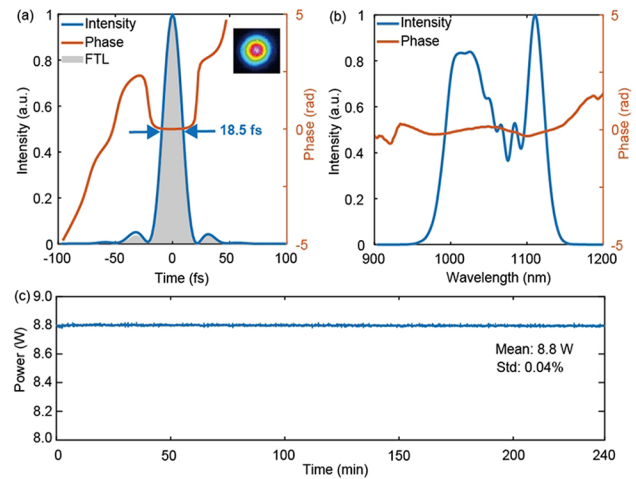


Fig. 3. First stage: MPC compression characterization. (a) Temporal and (b) spectral intensity (blue solid line) and phase (red solid line) characterization of the MPC output. FTL is displayed by a gray shadow in (a). (c) Output power stability over 4 h.

into two concave mirrors with a radius of curvature (ROC) of 300 mm. The distance of the two concave mirrors is about 50 cm, with two AR-coated fused silica (FS) plates of 1-mm thickness, which served as the nonlinear medium. The collimated beam after the MPC is compressed by a set of chirped mirrors. This compact system is integrated with a footprint of $55 \times 17 \text{ cm}^2$. Followed by the second spectrum broadening stage, the output beam from the MPC system is focusing by a concave mirror of 1500-mm ROC, with six FS plates of 0.1-mm thickness used as nonlinear media, which are placed with Brewster's angle, and the positions of FS plates are about -6 cm , -2 cm , $+2 \text{ cm}$, $+5 \text{ cm}$, $+8 \text{ cm}$, and $+10 \text{ cm}$ referring to the focus. The output beam is collimated by a concave mirror of 1000-mm ROC, the pulses are compressed by a set of chirped mirrors, and the over-compensated dispersion is fine-tuned by a set of FS wedges. The output beam is characterized by a SPIDER (FC SPIDER IR, APE GmbH) and an optical spectrum analyzer at 0.5-nm resolution (AQ6374E, Yokogawa).

Figure 3 shows the MPC output results. The mode matching process is carefully adjusted by inspecting the uniformity of the beam profile on a COMS-based beam profiler (LCM1310, DataRay) via leakage behind the concave mirror. As a result, the output beam quality is quietly good with Gaussian distribution. The output pulses from the MPC are compensated by introducing a -1600 fs^2 group delay dispersion (GDD) with eight bounces on a set of GTI mirrors (UltraFast Innovations GmbH). The measured pulse duration is 18.5 fs, approaching to FTL of 18.4 fs (Fig. 3(a)). The reconstructed temporal profile shows that over 92% of energy is contained on the mainlobe. The B-integral of each plate is estimated to be about 0.6 rad, resulting in spectrum spans of about 950 nm–1150 nm, and the corresponding phase is plotted in Fig. 3(b), which shows a quasi-flat phase. The input power before mode matching components and the MPC is 10 W, and the power stability is about 0.03%. The output power after GTI mirrors is 8.8 W, yielding a conversion efficiency of 88% and a peak power of 8.8 GW. The output power stability over 4 h is 0.04%. The output pointing stability is $13 \mu\text{rad}$ over 1 h against the input of $8.4 \mu\text{rad}$. The results show an 8-fold peak power boost and a nearly 10-fold compression.

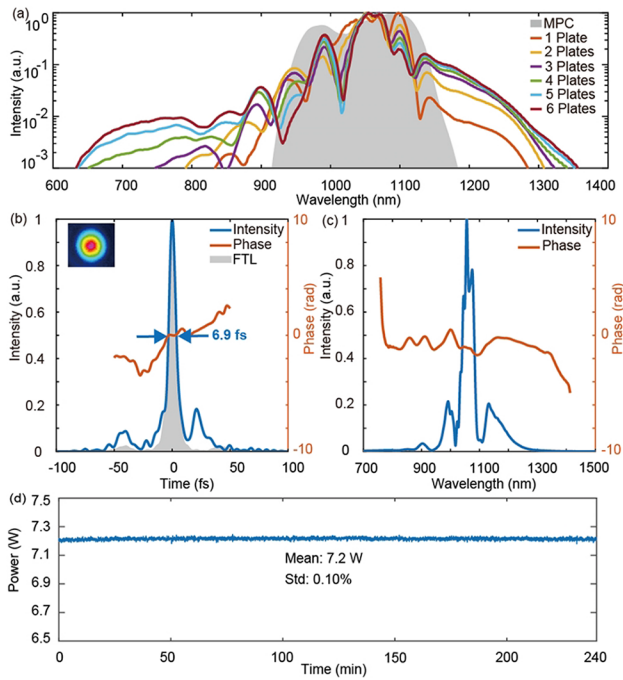


Fig. 4. Second stage: MTP compression characterization. (a) Output spectrum for different numbers of plates (solid lines) compared with the first MPC output (shadow area). (b) Temporal and (c) spectral intensity (blue solid line) and phase (red solid line) characterization of the MTP output with six plates. FTL is displayed by a gray shadow in (b). (c) Output power stability over 4 h.

To reach the few-cycle region, the second stage is applied by using the MTP approach. Figure 4(a) plots the dependence of the spectrum on the number of plates, compared with the MPC output. The spectrum is controlled from 630 nm to 1350 nm at the last plate, yielding an octave-spanning spectrum at -30 -dB level. The spectrum broadening process in this stage is dominated by self-phase modulation, since high order dispersion compensation will not be considered at the compression stage, and the self-steepening effect in this stage is controlled. The measured output pulses keep a high-quality Gaussian beam profile compared with the first stage output. The output pulses from the MTP are collimated by a 1000-mm ROC silver coated concave mirror and compensated by introducing a -240 -fs² GDD with four bounces on a set of chirped mirrors (UltraFast Innovations GmbH). The measured pulse duration is 6.9 fs with a FTL of 5.8 fs, resulting in two optical cycles at a center wavelength of 1030 nm (Fig. 4(b)). Note that only GDD compensation is performed in the compression stage. The reconstructed spectrum phase is plotted in Fig. 4(c), which shows slightly high order dispersion. The average power of compressed pulses is 7.2 W, with a power stability of 0.10% (RMS) over 4 h, yielding a throughput efficiency of 82% (Fig. 4(d)). The energy loss is mainly owing to the silver coated mirror behind the MTP and the irises. The reconstructed temporal profile shows that over 60% of energy is contained on the mainlobe, yielding the peak power of 12.5 GW. The overall peak power boost ratio is over 11.3 and the compression ratio is over 26. The output pointing stability is 20 μ rad over 1 h, and the degradation of power stability and pointing stability is mainly owing to the air fluctuation. Table 1 summarizes the performance of each stage compared with the laser input, including the FWHM pulse duration (τ_{FWHM}), pulse energy (E),

Table 1. Experimental Performance of Spectral Broadening and Compression in the First Stage and Second Stage Compared with the Laser Input

	Input	First Stage	Second stage
τ_{FWHM} (fs)	180	18.5	6.9
E (μ J)	200	176	144
P_{avg} (W)	10	8.8	7.2
P_{stab} (%)	0.03	0.04	0.10
η (%)	—	88	82
P_{peak} (GW)	1.1	8.8	12.5
σ (μ rad)	8.4	13	20
V_{avg} (%)	—	98.9	98.0

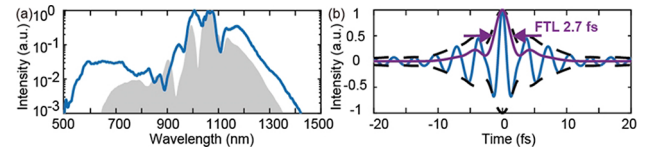


Fig. 5. (a) Spectrum comparison by changing the thickness of the last two plates as 0.2 mm (blue solid line) against the previous MTP setup (shadow area). (b) Fourier transform of the optimized spectrum, including the electric field (blue solid line), profile of electric field (black dashed line), and intensity profile (purple solid line).

average power (P_{avg}), power stability over 4 h in RMS (P_{stab}), efficiency in each stage (η), peak power (P_{peak}), pointing stability over 1 h (σ), and average spectral uniformity within $1/e^2$ intensity profile (V_{avg}). To conduct spectral homogeneity evaluation, a InGaAs based spectrometer (D-vision, Sphere photonics) and a 100- μ m pinhole are used, followed by the procedure described in [35]. The intensity weighted overlap average V-parameter within a $1/e^2$ horizontal intensity profile is 98.9% for the first stage and 98.0% for the second stage output. The data shows the proposed two-stage compression setup is a promising and efficient scheme to reach two-cycle pulses.

Moreover, our setup can further extend the spectrum since the spectrum broadening is not saturated yet by the previous MTP setup. By changing the position of the MTP and replacing the thickness of the last two plates from 0.1 mm to 0.2 mm, the position of the MTP is optimized about -4 cm, -1 cm, $+2$ cm, $+5$ cm, $+7$ cm, and $+9$ cm referring to the focus to get the saturation of the spectrum broadening. The final spectrum (blue solid line) compared with six FS with 0.1 mm (shadow area) is plotted in Fig. 5(a), where the optimized spectrum spans from 500 nm to 1420 nm, yielding a 1.5-octave-spanning supercontinuum at -30 -dB level. In this stage, the spectrum broadening process is dominated by self-steepening, as the asymmetric spectrum and the broader short wavelength extension compared with the long wavelength. In this case, high order dispersion is inevitable. Figure 5(b) shows the corresponding FTL results, where the blue solid line is the electric field, the black dashed line is the envelope of electric field, the purple solid line is the intensity with the FWHM of 2.7 fs, corresponding to 0.8 optical cycle at a center wavelength of 1041 nm, calculated by the center of gravity from the measured spectrum. The FTL intensity profile shows a peak power of 33 GW. We believed that by designing a chirped mirror with high order dispersion taken into consideration, the intense sub-cycle transient can be achieved.

In conclusion, we applied a compact all-solid-state MPC and MTP scheme to efficiently compress the output pulses from 180 fs down to 6.9 fs, enhancing the peak power from 1.1 GW to 12.5 GW and the long-term power stability of 0.1%. Our results reveal an efficient pathway to generate few-cycle pulses in all-solid state with superior long-term power stability. By optimizing the thickness and position of the FS plates on the second stage, we enhanced the self-steepening effect and extended the spectrum range to over 1.5 octave spanning, corresponding to 2.7-fs, 0.8-cycle FTL pulse duration. Furthermore, by using the second-harmonic generation and the residual fundamental pulses after the first stage, it is possible to further extend the white-light spectrum into a multi-octave-spanning regime by coherent combining two channel MTP systems [36,37].

Funding. National Key Research and Development Program of China (2020YFB1313702); Chinese Academy of Sciences Project for Young Scientists in Basic Research (YSBR-059); Beijing Natural Science Foundation for Distinguished Young Scholars (JQ22015).

Acknowledgment. S. Fang gratefully acknowledges support from Professor Mikio Yamashita, Professor Franz X. Kaertner, and Synergetic Extreme Condition User Facility (SECUF).

Disclosures. The authors declare no conflicts of interest.

Data availability. Data underlying the results presented in this Letter are not publicly available at this time but may be obtained from the authors upon reasonable request.

REFERENCES

1. M.-S. Tsai, A.-Y. Liang, C.-L. Tsai, *et al.*, *Sci. Adv.* **8**, eabo1945 (2022).
2. Y. Su, S. Fang, S. Wang, *et al.*, *Appl. Phys. Lett.* **120**, 121105 (2022).
3. S. Fang, T. Tanigawa, K. L. Ishikawa, *et al.*, *J. Opt. Soc. Am. B* **28**, 1 (2011).
4. A. P. Fidler, S. J. Camp, E. R. Warrick, *et al.*, *Nat. Commun.* **10**, 1384 (2019).
5. D. Nabben, J. Kuttruff, L. Stolz, *et al.*, *Nature* **619**, 63 (2023).
6. M. T. Hassan, *J. Phys. B: At., Mol. Opt. Phys.* **51**, 032005 (2018).
7. S. Li, L. Lu, S. Bhattacharyya, *et al.*, *Science* **383**, 1118 (2024).
8. D. A. Zimin, N. Karpowicz, M. Qasim, *et al.*, *Nature* **618**, 276 (2023).
9. D. Hui, H. Alqattan, S. Zhang, *et al.*, *Sci. Adv.* **9**, eadf1015 (2023).
10. D. Hui, H. Alqattan, S. Yamada, *et al.*, *Nat. Photonics* **16**, 33 (2022).
11. S. Zhou, C. Bao, B. Fan, *et al.*, *Nature* **614**, 75 (2023).
12. J. Wang, F. Chen, M. Pan, *et al.*, *Opt. Express* **31**, 9854 (2023).
13. F. Chen, J. Wang, M. Pan, *et al.*, *Rev. Sci. Instrum.* **94**, 043905 (2023).
14. Y.-G. Jeong, R. Piccoli, D. Ferachou, *et al.*, *Sci. Rep.* **8**, 11794 (2018).
15. Z. Pi, H. Y. Kim, and E. Goulielmakis, *Opt. Lett.* **47**, 5865 (2022).
16. M. Hanna, F. Guichard, N. Daher, *et al.*, *Laser Photonics Rev.* **15**, 2100220 (2021).
17. A.-L. Viotti, M. Seidel, E. Escoto, *et al.*, *Optica* **9**, 197 (2022).
18. M. Kaumanns, D. Kormin, T. Nubbemeyer, *et al.*, *Opt. Lett.* **46**, 929 (2021).
19. L. Silletti, A. Bin Wahid, E. Escoto, *et al.*, *Opt. Lett.* **48**, 1842 (2023).
20. J. Weitenberg, T. Saule, J. Schulte, *et al.*, *IEEE J. Quantum Electron.* **53**, 1 (2017).
21. S. Gröbmeyer, K. Fritsch, B. Schneider, *et al.*, *Appl. Phys. B* **126**, 159 (2020).
22. M. Seidel, P. Balla, C. Li, *et al.*, *Ultrafast. Sci.* **2022**, 9754919 (2022).
23. A.-K. Raab, M. Seidel, C. Guo, *et al.*, *Opt. Lett.* **47**, 5084 (2022).
24. A. Omar, M. Hoffmann, G. Galle, *et al.*, *Opt. Express* **32**, 13235 (2024).
25. K. Fritsch, M. Poetzlberger, V. Pervak, *et al.*, *Opt. Lett.* **43**, 4643 (2018).
26. E. Vicentini, Y. Wang, D. Gatti, *et al.*, *Opt. Express* **28**, 4541 (2020).
27. G. Barbiero, H. Wang, J. Brons, *et al.*, *J. Phys. B: At., Mol. Opt. Phys.* **53**, 125601 (2020).
28. S. Goncharov, K. Fritsch, and O. Pronin, *Opt. Lett.* **48**, 147 (2023).
29. S. Goncharov, K. Fritsch, and O. Pronin, *Opt. Lett.* **49**, 2717 (2024).
30. A.-L. Viotti, C. Li, G. Arisholm, *et al.*, *Opt. Lett.* **48**, 984 (2023).
31. J. E. Beetar, S. Gholam-Mirzaei, and M. Chini, *Appl. Phys. Lett.* **112**, 051102 (2018).
32. T. Okamoto, Y. Kunihashi, Y. Shinohara, *et al.*, *Opt. Lett.* **48**, 2579 (2023).
33. C.-L. Tsai, F. Meyer, A. Omar, *et al.*, *Opt. Lett.* **44**, 4115 (2019).
34. G. Barbiero, H. Wang, M. Graßl, *et al.*, *Opt. Lett.* **46**, 5304 (2021).
35. V. Hariton, K. Fritsch, K. Schwarz, *et al.*, *Opt. Express* **31**, 19554 (2023).
36. P. Huang, S. Fang, Y. Gao, *et al.*, *Appl. Phys. Lett.* **115**, 031102 (2019).
37. Y. Su, S. Fang, Y. Gao, *et al.*, *Appl. Phys. Lett.* **118**, 261102 (2021).